

Study of fast neutron detector for COSINE-100 experiment

COSINE-100 Collaboration

G. Adhikari^a, P. Adhikari^a, C. Ha^b, E.J. Jeon^b, K.W. Kim^b, N.Y. Kim^b, Y.D. Kim^{a,b}, Y.J. Ko^b, H.S. Lee^b, J. Lee^b, M.H. Lee^b, R.H. Maruyama^c, S.L. Olsen^b, and H. Prihadi^{b,d}

^a Department of Physics, Sejong University, Seoul 05006, Korea

^b Center for Underground Physics, Institute for Basic Science (IBS), Daejeon 34047, Korea

^c Department of Physics, Yale University, New Haven, CT 06520, USA

^d Department of Physics, Bandung Institute of Technology, Bandung 40132, Indonesia

E-mail: yjko@ibs.re.kr

ABSTRACT: A monitoring system for fast neutrons is planned in the COSINE experiment, a dark matter experiment with NaI crystals. We pursued several R&D approaches for a neutron detector using a liquid scintillator (LS). A pulse shape discrimination (PSD) technique is used for the identification of neutron events and the PSD properties of two different LS were compared. A good separation power between neutrons and γ has been achieved for energies between 200 keVee to 1500 keVee. The combination of alumina adsorption, filtration, and water extraction is effective in purifying the LS, which leads to a reduction in the α contamination by ^{210}Po of more than a factor of two. The measured activities of the internal α are 0.36 ± 0.04 mBq/kg and 0.21 ± 0.03 mBq/kg before and after purification, respectively.

KEYWORDS: Neutrons; COSINE-100 Experiment; Pulse shape discrimination; Dark Matter; Liquid Scintillator; NMD.

Contents

1. Introduction	1
2. Neutron Detector and Experimental Setup	2
2.1 Liquid Scintillator	3
3. Pulse Shape Discrimination	3
3.1 Energy Calibration of the Detector	3
3.2 PSD Parameter and Optimization	4
3.3 PSD Performance of Different Liquid Scintillators	5
4. Internal Alpha Background	6
4.1 Identification of Alpha Sources	6
4.2 Purification of the Liquid Scintillator	8
4.3 Plan for Main Detector	9
5. Summary	10

1. Introduction

The DAMA/LIBRA experiment, which has been operational for over 15 years, is an experiment to search for the evidence of dark matter scattering off nuclei using an array of ultra-low-background NaI(Tl) crystals [1]. DAMA/LIBRA consistently reports a positive signal with a significance of 9.3σ for an annual modulation [2, 3], and the signal is consistent with a weakly interacting massive particle (WIMP) that has a spin-independent nucleon cross section of approximately $2 \times 10^{-40} \text{ cm}^2$ [4].

The COSINE-100 experiment [5] has developed an ultra-low-background NaI (Tl) crystal detector [6, 7, 8] to search for WIMPs. The primary goal of the experiment is to confirm or refute the claimed observation of the DAMA/LIBRA experiment with the same type of crystal. The COSINE-100 experiment is located in the Yangyang Underground Laboratory (Y2L) with a minimum earth overburden of about 700 m [9]. There have been continuing debates about whether or not the DAMA/LIBRA annual modulation signal is due to muon-induced neutron signals that may have been seasonally modulated [10]. Therefore, it is important to understand the environmental neutron background for the COSINE-100 experiment.

In the case of fast neutrons, the energy conversion process is elastic scattering with light nuclei that gives rise to recoil nuclei. The main sources of neutrons are the spontaneous fission of ^{238}U in the rocks, (α, n) reactions caused by α particles from the decay of ^{238}U and ^{232}Th , and cosmic ray muons that split the target nuclei [11]. Highly energetic muons interacting with the shielding

materials can generate neutrons inside the shield. Since modulation of the environmental neutrons that can interact with nuclei is possible, neutron monitoring is necessary for the annual modulation study. In order to do that, we are constructing a neutron monitoring detector (NMD) using a liquid scintillator (LS), and it will be installed inside the main shielding of the COSINE detector. Here, we describe the R&D in the construction of the NMD for the COSINE-100 experiment.

2. Neutron Detector and Experimental Setup

A cylindrical vessel of 5-cm length and 4.5-cm inner diameter made of 1.5-cm thick Teflon is used for the neutron detector. An acrylic window of 10-mm thickness is attached to each end of the vessel with suitable O-rings to prevent leakage. Two different LSs are the candidates for the target of the neutron detector. One is based on Linear Alkyl Benzene (LAB) and the other is a commercial product called “Ultima Gold-F (UG-F)” based on Di-isopropylnaphthalene (DIN; $C_{16}H_{20}$). The test detector is read out by two 3-inch photomultiplier tubes (PMT; Hamamatsu R12669SEL) mounted on each end of the cylinder. The PMTs have bi-alkali photocathodes that have 35% maximum quantum efficiency at a wavelength of around 420 nm.

The flash ADC, which has a 12-bit resolution with 500 MHz sampling, records the digitized signal waveforms from the anode readout of two PMTs. We use the logic "AND" of the signals from the two PMTs to form a trigger signal. Only when both PMTs simultaneously have signals above the threshold are the waveforms recorded. The trigger threshold is set at 9.2 mV when two channels coincide within a 64 ns window. The SY4252 CAEN module is used to supply the high voltage on PMTs. In order to reduce environmental neutrons and γ , the detector was surrounded by 5-cm thick polyethylene (PE) and a 5-cm thick normal lead shield in the test setup, as shown in Fig. 1.

There is another similarly configured detector with a ten times larger volume to understand the background level. The detector is installed inside the KIMS-CsI shielding test facility at the



Figure 1. Experimental setup for the PSD of the neutron detector.

Y2L [12]. The available polyethylene shielding may be good enough to prevent external neutrons so that neutron-like events in the α band are assumed to be negligible.

2.1 Liquid Scintillator

We chose LAB as the base solvent material. LAB has several advantages as follows:

- Light yield comparable with pseudocumene.
- High flash point (approximately 130°C).
- Long attenuation length (> 10 m at 430-nm wavelength) [13].
- Domestically available.
- Relatively safe material.

The emission spectrum of LAB has a maximum at 340 nm, so we mix the solvent with the wavelength shifter to adjust the wavelength of the optical photons to be suitable for the PMT. We used the neutrino grade of the 2,5 diphenyloxazole (PPO; $C_{15}H_{11}NO$) for the primary fluor and the scintillation grade of the 1,4-bis(2-methylstyryl)benzene (bis-MSB; $(CH_3C_6H_4CH=CH_2)_2C_6H_4$) for the secondary wavelength shifter. The amount of PPO was chosen to be 3 g/L and of bis-MSB was chosen to be 30 mg/L [14].

The commercial LS cocktail produced by PerkinElmer company known as “Ultima Gold-F,” which has a higher flash point (approximately 150°C), is also studied. DIN is a solvent for this cocktail. In comparison to cocktails based on DIN, the classical cocktails show very short pulse lengths [15]. The discrimination is much easier if the pulses are extended. As UG-F is a commercial LS, the type and quantity of the wavelength shifter mixed into the DIN solvent were not clear.

3. Pulse Shape Discrimination

3.1 Energy Calibration of the Detector

The detector was calibrated with 1332-keV γ from ^{60}Co . Since it is difficult to find the full peak of the ^{60}Co charge distribution due to the small size of the detector, the Compton edge, 1122 keV for 1332 keV γ , was used for the energy calibration. The following function is used for fitting the charge distribution to estimate the energy of the Compton edge:

$$f(q) = \frac{p_0}{\exp[p_1(q - p_2)] + 1}, \quad (3.1)$$

where the p_i s are the fitting parameters and q is the charge. In this equation, p_2 denotes the energy of the Compton edge. Fig. 2 shows the charge distribution of the γ events from ^{60}Co and the fitted function.

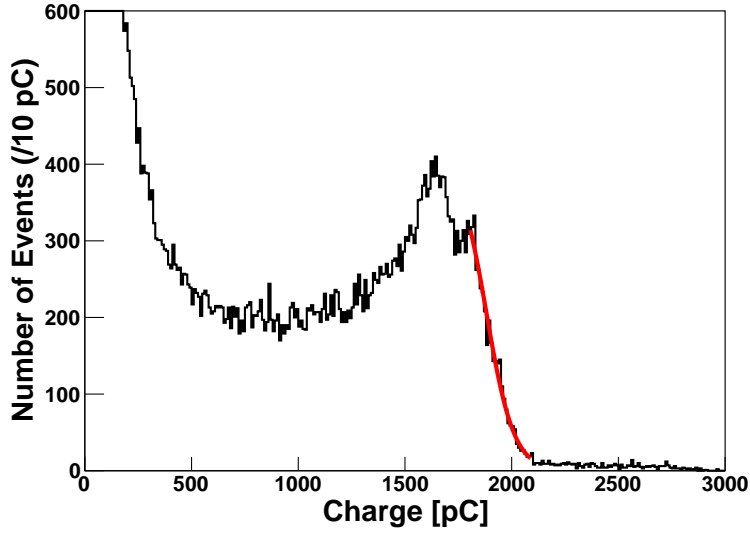


Figure 2. Charge distribution of γ events from ^{60}Co for energy calibration. The red line is a fitted function to estimate the energy of the Compton edge of 1332 keV γ from ^{60}Co . Both Compton edges of 1332 keV and 1172 keV γ are superimposed as a single Compton edge.

3.2 PSD Parameter and Optimization

When a particle deposits its energy in the LS, it excites the solvent molecules, which causes chemical quenching. The energy of the solvent molecules is transferred to the fluor molecules, and optical photons emitted from the fluor molecules are received by the photocathode of the PMT. The light emitted from the vast majority of the organic LS consists of two main components: the fast and the slow components. The fast one has an exponentially decaying lifetime that is typically in the range of a few nanoseconds. The slow component has an exponential tail extending out to several hundred nanoseconds [16]. The relative intensities of the two components depend on the specific energy loss of the particle passing through the LS.

Fast neutrons deposit their energies via proton recoil while γ deposit their energies via electron recoil. The energy losses of the proton and the electron are different, so the signal shape of fast neutron events is different from that of γ events, as shown in Fig. 3 (a). The signal shape of proton recoil has a longer tail than that of electron recoil due to greater de-excitation of different states in the LS [17]. Therefore, the γ and neutron events can be distinguished via their signal shape.

For particle identification, the tail charge Q_{tail} is defined as

$$Q_{\text{tail}} = \int_{t_c}^{t_{\text{max}}} \frac{V(t)}{R_{\text{terminal}}} dt, \quad (3.2)$$

where $R_{\text{terminal}} (= 50 \Omega)$ is the terminal resistance and the range $[t_c, t_{\text{max}}]$ is the tail section. The γ and neutron events can be separated using the ratio between the tail charge Q_{tail} to the total charge Q_{total} ; thus, this ratio is used as a PSD parameter.

The starting time of tail section, t_c is optimized to get highest separation power between the γ and neutron bands via neutron calibration data. The separation power is quantitatively expressed

in terms of the figure of merit (FoM) as follows:

$$\text{FoM} = \frac{|m_n - m_\gamma|}{\sqrt{\sigma_n^2 + \sigma_\gamma^2}}, \quad (3.3)$$

where m_n (m_γ) and σ_n (σ_γ) represent the mean and standard deviation of the PSD distribution of the neutrons (γ s), respectively. The higher FoM indicates better discrimination between events induced by γ and neutron. Therefore, we select the t_c to be 36 ns because the FoM has the maximum value at $t_c = 36$ ns from the maximum pulse bin, as shown in Fig. 3 (b).

3.3 PSD Performance of Different Liquid Scintillators

The LS is filled into the container as described in Sec. 2. If there are oxygen molecules in the LS, since they may remain between the scintillating molecules, they can lower the light output and degrade PSD performance. In order to control the oxygen quenching, we fill the LS into the container in an oxygen-free environment inside the glove box. The separation power between

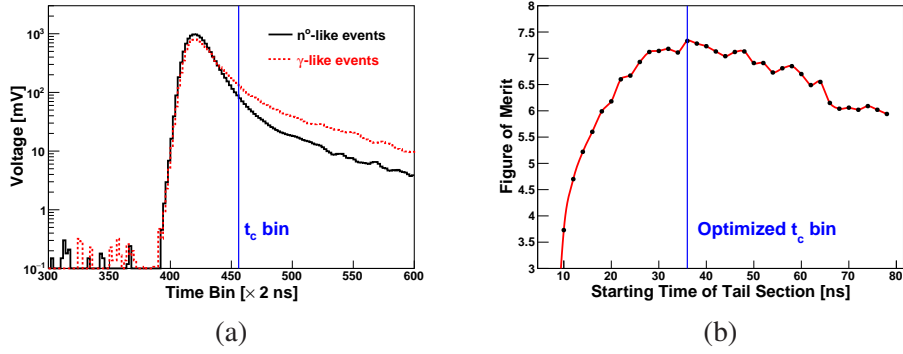


Figure 3. (a) Signal shape of neutron and γ events in UG-F. (b) Optimization of starting time of the tail section, t_c .

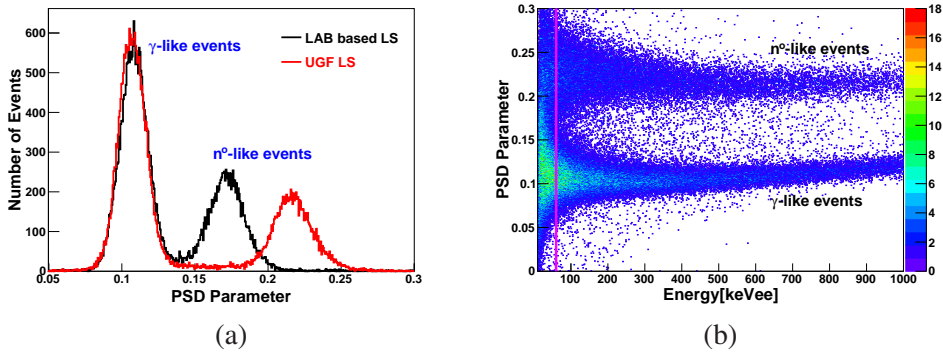


Figure 4. (a) Comparison of the PSD parameter distributions of LAB- and DIN-based (UG-F) LSs in the energy range [200, 1000] keVee, and (b) scatter plot between the PSD parameter and energy in the case of the UG-F. The magenta line shows the PSD threshold.

neutron and γ events from a ^{252}Cf source is compared between the samples via the technique described in the previous section. In this comparison, the Q_{tail} is optimized for each sample and the PSD parameter works well for both samples, as shown in Fig. 4 (a).

The FoM of UG-F is measured to be 7.1 in the energy range [200, 1000] keVee, while the LAB-based LS shows an FoM of 4.01 measured in the same energy range. The PSD threshold is approximately 70 keV with a 3.1 FoM for the small 70 ml R&D detector, as shown in Fig. 4 (b). So, we expect acceptable an FoM and PSD threshold for the COSINE NMD having mass of about 5 kg. Based on the PSD performance, UG-F is a better candidate material for the NMD.

4. Internal Alpha Background

Since the energy loss of an α particle is similar to that of a proton, α events cannot be distinguished from neutron events via PSD. It means that the internal α background will give rise to uncertainties in the neutron rate measurement, so understanding the α background and reducing it as much as possible is very important for neutron measurements. In order to understand the background, a detector filled with UG-F having a volume of approximately 700 ml is installed inside the KIMS-CsI shielding test facility at the Y2L.

4.1 Identification of Alpha Sources

In Sec.3, the DIN-based LS (UG-F) is selected for the NMD, thus the activity of the internal α from the UG-F are measured at the Y2L. Since the PSD of α events is similar to that of neutron events, the α events can be identified via the PSD from β/γ events. In Fig.5, one can see a band and several islands. The band denotes β/γ events, and the islands are α events.

The α - α coincidence between ^{222}Rn and ^{218}Po decay and β - α coincidence between ^{214}Bi to ^{214}Po decay can be identified because of their fast lifetimes [7, 12]. Fig. 6 shows the distribution

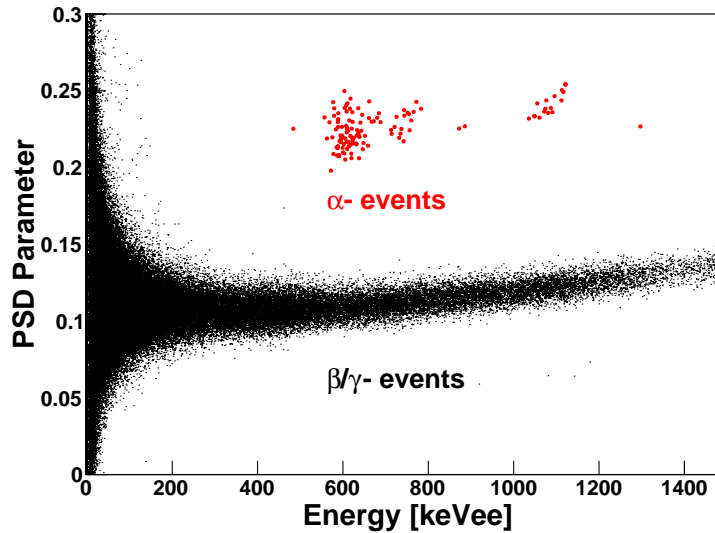


Figure 5. Scatter plot between PSD parameter and electron -equivalent energy for background data

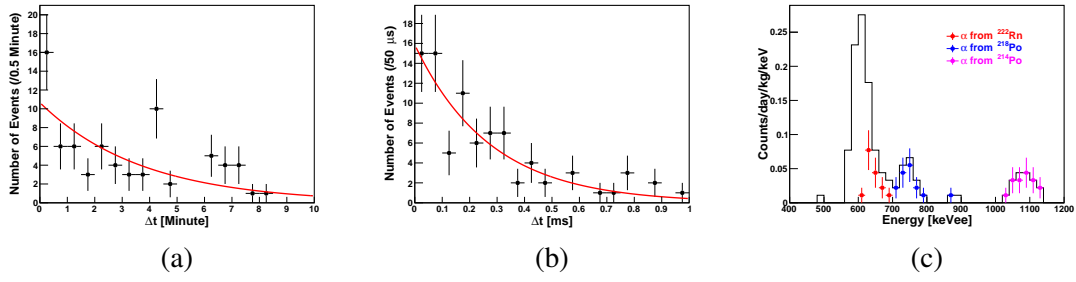


Figure 6. (a) Time difference distribution between two α events from ^{222}Rn and ^{218}Po . (b) Time differences between β and α events from ^{214}Bi and ^{214}Po , respectively. The red curves in (a) and (b) are an exponential function fitted to the time difference. (c) Energy distribution of the α events.

of the measured time intervals between two successive α - α and β - α induced events. The lifetime estimated from the fitting of ^{218}Po is 2.6 ± 0.5 min, and that of ^{214}Po is obtained as $191 \pm 26 \mu s$, which are consistent with the known values. The red and blue dots in Fig.6 (c) show the energy distributions of tagged α events from ^{222}Rn and ^{218}Po , respectively. Likewise, the magenta dots in Fig.6 (c) show the energy distributions of tagged α events from ^{214}Po .

Similarly, we can identify an α - α coincidence with a half-life of 145 ms between ^{220}Rn to ^{216}Po in the ^{232}Th decay chain. However, the number of events after applying the selection criteria is too small to fit, so we calculated conservatively and obtained an upper limit of 0.01 mBq/kg.

The α energy distribution cannot be fully explained by the α sources identified by the timing analysis. Since the α source that has α energy slightly less than the 5.59 MeV of ^{222}Rn should be

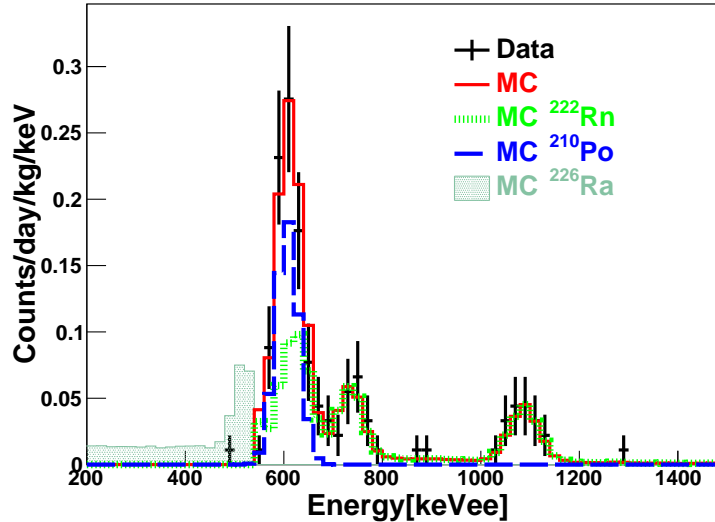


Figure 7. Energy distributions of measured (black) and simulated (red) α events. The red line includes the decay chain of ^{222}Rn and α events from ^{210}Po (blue line). The filled area indicates only α events from ^{226}Ra .

added, a decay chain and a α -decay are simulated. The first one is the decay chain beginning with ^{226}Ra that decays into 4.87-MeV α and ^{222}Rn , and the other is ^{210}Po , which decays into ^{206}Pb and 5.41-MeV α . As shown in Fig.7, the remaining component can be assumed to be ^{210}Po , and there are no α events from ^{226}Ra . This means the possibility of UG-F contamination by the ^{222}Rn , so we take data for 13 days, considering the half-life of ^{222}Rn . However, the total α rate is stable during the measurements; therefore, the LS is contaminated by the ^{210}Po . The activities of all components are presented in the next section, including a comparison with those of the purified sample.

4.2 Purification of the Liquid Scintillator

Purification of the liquid scintillator is a well-known method to reduce the internal α background of the liquid scintillator. The combination of alumina adsorption and water extraction is studied for the UG-F liquid scintillator. The adhesion of impurities from a liquid to a solid surface is the basic principle of adsorption. Aluminum oxide, which is an adsorbent, is effective at removing impurities for metals and ions and has been successfully used for scintillator purification [18]. Alumina powder of 45- μm grain size and the UG-F are mixed, and are then separated by vacuum filtration using a PTFE membrane filter with a 0.25- μm pore-size. The sample after alumina adsorption is purified once more by water extraction and nitrogen purging before the measurement. When two immiscible solvents like water and LS are brought into close phase contact, impurities present in the LS that are more soluble in water can be transferred to the water from the LS. Thus, we obtain a purified LS after re-separating. For the process of water extraction, the LS and the ultra-pure DI water having a 16.4 M Ω resistance are mixed into the container at a ratio of 4:1, respectively. After mixing, the mixture is stored for a day in order to separate the water and LS. The LS and water layers are separated using a separation funnel. Following water extraction, the LS is filled into the container after nitrogen purging to remove radon contamination during the purification process.

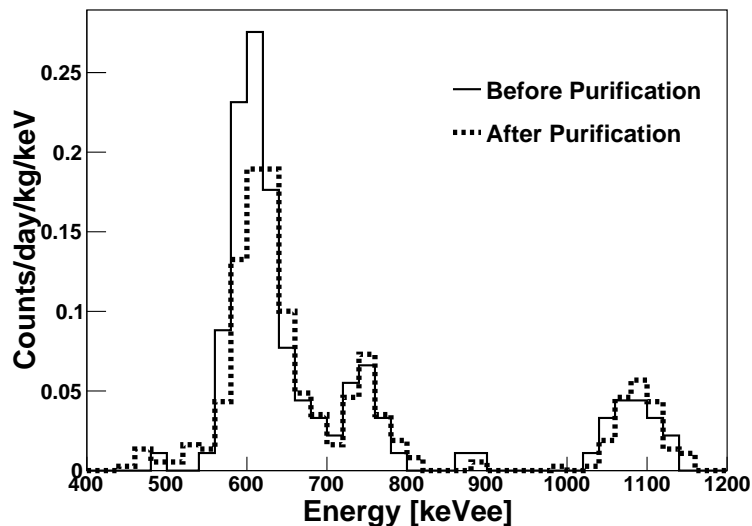


Figure 8. Comparison of the internal α energy distribution before (black) and after purification (red)

Sample	^{222}Rn	^{218}Po	^{214}Po	^{210}Po	Total α
ND-1	0.030 ± 0.007	0.030 ± 0.007	0.041 ± 0.008	0.25 ± 0.02	0.36 ± 0.04
ND-2	0.025 ± 0.003	0.025 ± 0.003	0.032 ± 0.004	0.12 ± 0.007	0.21 ± 0.03

Table 1. Activities of all α components with the UG-F before (ND-1) and after (ND-2) purification. All units are mBq/kg.

Since the LS contamination is estimated to be mostly due to ^{210}Po in Sec. 4.1, the LS purification is expected to mainly reduce ^{210}Po . We analyze the α events of the sample after purification via the same method in Sec. 4.1, and the activities are summarized in Table 4.2. In the table, ND-1 and ND-2 are the UG-F samples before and after purification, respectively. As expected, the activity of the ^{210}Po is reduced by more than twofold and other components did not show any significant differences compared to their errors. Fig.8 shows the energy distributions of the α events before and after purification.

4.3 Plan for Main Detector

For the main detector, the vessel to be filled with the LS is designed as a cylindrical homogeneous type made of Teflon with a thickness of 1.5 cm. A homogeneous type has advantages over a segmented type because spaces and walls between segments may degrade detection efficiency or lose scintillation photons, which may worsen the resolution. Due to its higher reflectance, Teflon is considered as the body of the detector so that we do not need to use any extra materials to increase light collection efficiency as a reflector. Transparent acrylic windows with a thickness of 1 cm are coupled to both ends of the detector with O-rings to prevent the LS from leaking. With limited available space, the target size is decided to be 40 cm in length and 13 cm in diameter. As a result, the total target volume is about 6 l. Two PMTs are coupled at both ends using optical grease and fixed using Teflon cover end-caps with a Teflon guide, as shown in Fig. 9. The detector is surrounded by dark sheets to prevent light leaking in. The detector will be installed inside the main shielding of the COSINE detector.

The detector will be made very soon, and then the detector response, including PSD properties, will be studied. After understanding the detector performance, it is going to be installed inside

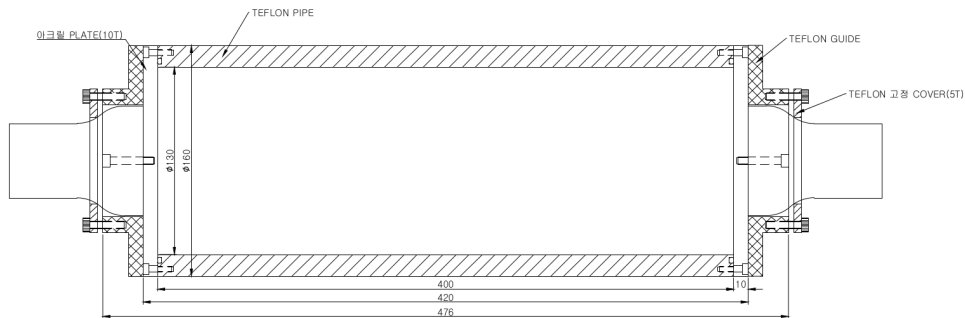


Figure 9. Design of the COSINE Neutron Monitoring Detector

the shielding of the COSINE detector in the near future. We will also install a similar type of detector outside of the main shielding to monitor the fast neutron flux. The detectors will be used to understand the neutron sources and to study the effects by neutrons in the DAMA annual modulation study.

5. Summary

The LAB- and DIN-based LSs were tested in terms of their PSD properties to select the target material of the main detector, and the DIN-based LS, UG-F, is selected due to its better PSD performance compared to that of the LAB-based LS. We recorded the data with a prototype neutron detector inside the shielding of the KIMS-CsI at the Y2L to measure the internal α background. The activity of the total α events was measured to 0.36 ± 0.04 mBq/kg, and the LS contamination is estimated to be almost entirely caused by ^{210}Po . The purification process of the LS including water extraction and alumina adsorption was tested, and the activity of the ^{210}Po decreased from 0.25 ± 0.02 mBq/kg to 0.12 ± 0.007 mBq/kg.

Acknowledgments

We thank the Korea Hydro and Nuclear Power (KHNP) Company for providing the underground laboratory space at Yangyang. This work is supported by the Institute for Basic Science (IBS), Republic of Korea, under project code IBSR016-A1.

References

- [1] R. Bernabei *et al.*, *New results from DAMA/LIBRA*, *Eur. Phys. J. C* **67** (2010) 39
- [2] R. Bernabei *et al.*, *Final model independent result of DAMA/LIBRA-phase 1*, *Eur. Phys. J. C* **73** (2013) 2648.
- [3] R. Bernabei *et al.*, *No role for muons in the DAMA annual modulation results*, *Eur. Phys. J. C* **72** (2012) 2064.
- [4] C. Savage *et al.*, *Compatibility of DAMA/LIBRA dark matter detection with other searches*, *J. Cosmol. Astropart. Phys.* **04** (2009) 039.
- [5] G. Adhikari *et al.*, *Initial performance of the COSINE-100 experiment*, *Eur. Phys. J. C* **78** (2018) 107.
- [6] K.W. Kim *et al.*, *Tests on NaI(Tl) crystals for WIMP search at Yangyang Underground Laboratory*, *Astropart. Phys.* **62** (2015) 249.
- [7] P. Adhikari *et al.*, *Understanding internal backgrounds in NaI(Tl) crystals toward a 200 kg array for the KIMS-NaI experiment*, *Eur. Phys. J. C* **76** (2016) 185.
- [8] G. Adhikari *et al.*, *Understanding NaI(Tl) crystal background for dark matter searches*, *Eur. Phys. J. C* **77** (2017) 437.
- [9] H. Prihtiadi *et al.*, *Muon detector for the COSINE-100 experiment*, *JINST* **13** (2018) T02007.
- [10] Blum K, *DAMA vs. the annually modulated muon background*, *astro-ph.HE arXiv:1110.0857* (2011).

- [11] J. W. Kwak *et al.*, *Performance of a Large Volume Liquid Scintillation Detector for the Measurement of Fast Neutrons*, *Journal of the Korean Physical Society*, **47** (2005) 202-206
- [12] H. S. Lee *et al.*, *Development of low background CsI(Tl) crystals for WIMP search*, *Nuclear Instruments and Methods in Physics Research A*, **571** (2007) 644-650.
- [13] Ding Y *et al.*, *A new gadolinium- loaded liquid scintillator for reactor neutrino detection*, *Nuclear Instruments and Methods in Physics Research A* **584** (2008) 238-243.
- [14] J. S. Park *et al.*, *Production and optical properties of Gd-loaded liquid scintillator for the RENO neutrino detector*, *Nuclear Instruments and Methods in Physics Research A*, **707** (2013) 45-53.
- [15] Song *et al.*, *Feasibility study of a gadolinium-loaded DIN-based liquid scintillator*, *Journal of the Korean Physical Society* **63** (2013) 970.
- [16] R. L. CRAUN *et al.*, *Analysis of response data for several organic scintillators*, *Nuclear Instruments and Methods*, **80** (1970) 239-244.
- [17] Paolo Lombardi *et al.*, *Decay time and pulse shape discrimination of liquid scintillators based on novel solvents*, *Nuclear Instruments and Methods in Physics Research A*, **701** (2013) 133-144.
- [18] J. Ford *et al.*, *Purification of Liquid scintillator and Monte Carlo simulation of relevant internal background in SNO+ , A thesis submitted to the Department of Physics, Queen's University, Canada* (2008).